Chapter 14. Tides, Earthquakes and Volcanic eruptions

Stéphanie Dumont[1], Susana Custódio[2], Simona Petrosino[3], Amanda M. Thomas[4] , Gianluca Sottili[5]

1 Instituto Dom Luiz (IDL), Universidade da Beira Interior, Covilhã, Portugal
2 Instituto Dom Luiz (IDL), Faculdade de Ciências, Universidade de Lisboa, Lisboa, Portugal
3 Istituto Nazionale di Geofisica e Vulcanologia, Sezione di Napoli – Osservatorio Vesuviano, Naples, Italy
4 Department of Earth Sciences, University of Oregon, Eugene, Oregon, USA
5 Dipartimento di Scienze della Terra, Sapienza-Università di Roma, Rome, Italy

1. Introduction

Earth tides result from gravitational pull forces caused by celestial bodies and their motion, of which the Moon and the Sun are the most relevant to our planet. The most striking expression of tides is the sustained ebb-and-flow of the ocean. Tides strongly affect the free masses that compose the fluid envelopes of the Earth and generate ocean and atmospheric tides (see chapters 4 and 16), but they also affect the solid Earth by generating solid Earth tides. This lunisolar gravitational force is also known for influencing the Earth's rotation (see chapter 17), resulting in a mass redistribution that induces a relative reorganization of stresses at the surface of the solid Earth (Lambeck, 2005; Le Mouël et al., 2019; Lopes et al., 2021).

The idea that ocean loading, which corresponds to the displacement from mass loading due to ocean tides, could trigger earthquakes can be tracked back to the 17th century (Emter, 1997). An abundance of observations and investigations followed in the early and mid-twentieth century, reporting possible tidal triggering of earthquakes at regional and global scales. The number of studies published per year on the relationship between tides and earthquake and volcanic activity has since steadily increased, from less than 10 before the 1970s to over 100 after 2010, accompanying closely the growing trend in the number of studies on earthquakes and volcanoes itself (**Figure 14.1, inset**). These observations have been extended to volcanic eruptions and more generally to measurements of volcanic and seismic activity (Mauk and Johnston, 1973; Emter, 1997 and references therein; Sottili et al., 2021).

Fluids, and more specifically pore fluid pressure, are known to play an important role in the behavior of rock failure. Pore fluid pressure is a key parameter in the well-known Coulomb failure criterion, whose variations may influence the initiation of earthquake rupture (Scholz, 2019). In continental fault systems, these fluids are usually related to groundwater, which mix with saline waters in marine and coastal environments. The link between seismic activity and fluids starts at the microscopic scale with pore pressure and extends to a regional scale with ocean loading. The oscillation of the ocean in response to Earth tides induces pressure and hence stress changes. These tidal variations are much smaller (~10^{-3} – 10^{-2} MPa, Cochran et al., 2004) than the strength of rocks and faults, (~10^{-1}-10^{3} MPa, Scholz, 2019). This has fueled the debate on the role of tidal influence on seismic and volcanic activity.

However, tides may have a larger impact than anticipated at first. Stress builds up slowly along crustal fault systems, at time scales of hundreds to thousands of years. Variations in the frictional behavior, together with recurring slip instabilities along the fault plane, can make the fault locally unstable (Scholz, 2019). Under these conditions, even small perturbations, such as those due to tidal stresses may initialize rupture and resulting dynamic stress changes can help to sustain rupture generating larger earthquakes (Ide et al., 2016).

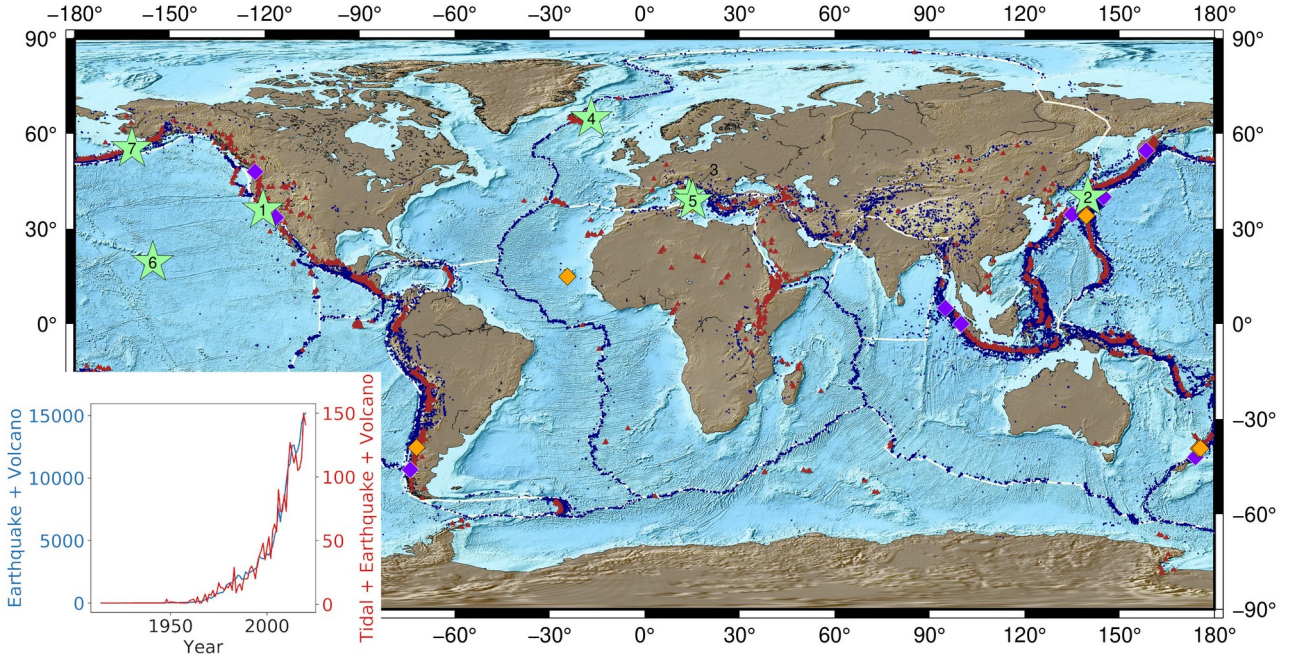

Figure 14.1: Global distribution of seismicity (blue dots) and volcanoes (garnet triangles). The green stars indicate locations of case studies in the chapter -- (1) San Andreas fault, California; (2) Japan subduction zone, (3) Campi Flegrei caldera, Italy, (4) Holuhraun eruption, Iceland; (5) Stromboli volcano, Italy; (6) Kilauea, Hawaii and (7) Pavlof volcano, Alaska. The purple and orange diamonds represent tectonic and volcanic settings listed in **Table 14.1 and Table 14.2** respectively, with evidence of tidal influence on seismic and volcanic activity. In the inset, the blue line shows the total number of articles published per year containing the words "earthquake" or "seismicity" or "volcano" or “eruption” in the abstract, whereas the red line shows the number of articles per year containing “tidal” or “tides” in the abstract in addition to the previous words. Data obtained from SCOPUS (https://www.scopus.com).

At land and submarine volcanoes, fluids act from the microscopic to regional scale, with a role that is strengthened by the presence of magma. In addition to modifying the mechanical behavior of rocks, magma forms a fantastic source of energy that is partly dissipated by rock, and more importantly by groundwater and gas emission. As a result, most active volcanoes are associated with hydrothermal systems that are formed by a mixture of groundwater and hot magmatic fluids. The gas species present in these fluids are progressively released according to their pressure-dependent solubility and convect within the surrounding porous medium. Gas escape is generally facilitated at volcanoes with (semi) permanent conduits; these are known as open systems. When conduits are sealed, the gas release is prevented and volcanic systems are referred to as closed. Consequently, volcanic systems may undergo large pressure changes. The variations in pore fluid pressure that accompany those of heat flux may result in the pressurization of the hydrothermal system that resides above the magma storage zone. This pressurization may eventually lead to a critical state prior to eruption triggering. The physico-chemical processes governing the dynamics of volcanic systems are inherently pressure-dependent, hence volcanic systems are sensitive to a wide range of pressure variations, beginning with small tidal stress variations.

Earth tides can therefore act as an external forcing on seismic and volcanic activity, by inducing changes in the dynamical state of faults and volcanoes. Tidal oscillations add in intricacy to the already complex internal processes of these geological objects. In this compounded framework, several approaches have been proposed to identify tidal influences on seismic and volcanic activity. Notably, deciphering the interplay between external and internal processes at different time scales

can provide key insights on the conditions leading to the triggering of earthquakes and volcanic eruptions.

In this chapter, we will review the diverse observations and methodologies that have been used to demonstrate the tidal influence on seismic and volcanic activity. We will then provide examples of well-documented tectonic and volcanic systems where this influence has been clearly observed. Finally, we will provide insights on why some geological systems seem to be sensitive to the small tidal strains and stresses.

2. Data and methods to study the tidal influence on faults and volcanoes

2.1 Observations

Geophysical and geochemical observations contribute to our understanding of the processes that affect faults and volcanoes, as well as their interactions. The acquisition of data during earthquakes and volcanic eruptions is essential but data collection during those periods alone is not sufficient to understand their triggering. It is the long-term acquisition of data, especially when faults and volcanoes are quiescent, that allows to define their background activity and the subdued phases of unrest and conditions that may lead to an earthquake or eruption.

Numerous studies have shown that the occurrence and rate of earthquakes (**Table 14.1 and Table 14.2**) are correlated with both solid Earth and ocean tides (Emter 1997; Tanaka et al., 2004, 2012; Ide et al., 2016; Shebalin and Baranov, 2020). This response to tidal stresses has been mainly evidenced for shallow (<90 km) earthquakes (Tanaka et al. 2004, 2012; Ide et al., 2016; Petrosino et al., 2018; Shebalin and Baranov, 2020), but also before or after large earthquakes (Mw ≥5, Tanaka et al., 2012; Shebalin and Baranov, 2020) and similarly, prior to volcanic eruptions (Girona et al., 2018).

Unlike the strong shaking caused by earthquakes, slow slip events may last several months and have slip speeds that are orders of magnitude lower than typical earthquakes. These slow earthquakes represent shear slip on the tectonic plate interface and are often accompanied by a weak seismic signal known as low-frequency earthquakes (LFEs). These are small magnitude earthquakes that are depleted in high-frequency content (i.e., ≥10 Hz). LFEs often occur in rapid succession making up tectonic tremor an emergent, low-amplitude, sustained seismic signal. While slow slip events relate to slip along the plate interface, tremor can also be generated by the movement of fluids and is detected in a variety of settings, especially in volcanic environments where magmatic and hydrothermal fluids can coexist (**Table 14.1 and Table 14.2**). When studying tremor, seismologists typically consider the seismic amplitudes in specific frequency bands (e.g., 1-10 Hz). The analysis of their temporal evolution reveals clear modulations with diverse tidal periodicities, from semi-diurnal to semi-annual **(Table 14.1 and Table 14.2)**, which are also detected in tremor recorded during volcanic eruptions (Custódio et al., 2003; Thomas et al., 2009, 2012; Ide et al., 2014; Royer et al., 2015; Girona et al., 2018; Dumont et al., 2020, 2021). Moreover, crustal properties are also influenced by tides as illustrated by studies on seismic noise and repeating earthquakes. Hillers et al., (2015) and Malagnini et al., (2019) showed that seismic velocities and attenuation oscillate at tidal

frequencies as a result of fluctuations in density of micro cracks and pore-fluid saturation within fault zones.

At quiescent volcanoes, activity is restricted to scarce seismic swarms and sustained hydrothermal activity, which may take the form of elevated temperatures and fumaroles at the ground surface. Similar to gas emissions at open-vent volcanoes, all these phenomena seem to be influenced by solid Earth and ocean tides, as illustrated in **Table 14.2** (Bredemeyer and Hansteen, 2014; De Lauro et al., 2018; Petrosino et al., 2018; Caputo et al. 2020). During eruptions, the influence of tides has been documented by variations of seismic tremor, thought to indicate the movement of magmatic fluids from the upper crust to the surface, variations of gas fluxes, and energy radiated by growing lava fields (Dumont et al., 2020, 2021). Moreover, tidal strain can accelerate pressure accumulation/release in volcanic conduits, as suggested by the detection of semi-diurnal and diurnal periods in ground tilt measurements and seismic bursts during the 2000 Miyake-Jima eruption in Japan (Kasahara et al., 2001). Some studies have also correlated the occurrence of volcanic eruptions with specific lunisolar cycles, in particular with the fortnightly tide, Mf, as documented for eruption onsets at Kilauea volcano, Hawaii, or Stromboli, Italy (Dzurisin, 1980; Sottili and Palladino, 2012).

Finally, the analysis of global catalogs of earthquakes and volcanic eruptions tends to confirm the observations made at local and regional scales. Based on 680 major eruptions that occurred between 1900 and 1971, Mauk and Johnston (1973) showed that the highest probability for an eruption to start was at times of maximum fortnightly amplitude. Although submarine eruptions at mid-oceanic ridges are also sensitive to the fortnightly cycle, they mainly initiate at neap tides, which correspond to a minimum in the fortnightly amplitudes (Tolstoy et al., 2015). Actually, this configuration of quadrature, i.e., when the Moon-Earth axis is perpendicular to the Sun-Earth axis, is associated with a minimum in ocean loading, a condition that favors the triggering of submarine eruptions. The maximum of ocean loading and amplitude variations are reached during syzygies, i.e., at the alignments of the Moon, Sun and Earth, and have a higher impact on subaerial systems like coastal and insular environments (Dzurisin, 1980; Sottili and Palladino, 2012). Long variations of ocean loading may also affect the dynamics of these subaerial systems as revealed by McNutt and Beavan (1987) for Pavlof volcano, Alaska. Ocean tides have been more systematically considered when investigating correlations between tidal stresses and specific seismic events (Tanaka et al., 2004, 2012; Ide et al., 2014, 2016), whereas their influence on global earthquake catalogs is more debated. Although data selection and catalog completeness may bias the studies of tidal influence, other factors and processes influence these dynamical systems, including specific properties of the systems, such as local tectonic stresses. Thus, while some studies have found a tidal control for large seismic events associated with shallow strike-slip and reverse faulting (Cochran et al., 2004), others have not confirmed such relationship for Mw>7.5 earthquakes (Kossobokov et al., 2020).

Tectonic setting (period of activity)	Region (Large event)	data/parameter	Method	Correlation with	Detected tides	Referenc
Transform (before & after LE)	San Andreas Fault USA (2004, Mw 6)	Seismic attenuation	Periodogram; statistics		*LT:* Sa, polar and multi-annual tides, fortnightly	Malagnini e 2019
Transform	San Andreas Fault USA	Rate of non-volcanic tremor and low-frequency earthquakes	Schuster test	Theoretical solid and ocean tides	*ST:* M2, N2, K2, K1, O1, P1, Q1, S2	Thomas et 2009; 201
Transform	Pinon Flat Observatory, USA	Seismic noise (2 - 8 Hz) /seismic velocity variations	correlation	Theoretical tidal strain; groundwater well and meteorological data		Hillers et al.,
Compressional (subduction, before LE)	Tohoku-Oki (2011, Mw 9.0)	Seismicity (< 70 km, Mw >=5)	Schuster test	Theoretical tidal stresses and ocean loading*		Tanaka et al.,
Compressional (subduction)	Japan (M >=2)	Seismicity (< 70 km)	Statistical test	Theoretical tidal stresses and ocean loading*		Tanaka et al.
Compressional (subduction)	Sumatra (2004, Mw 9.3); Chile (2010, Mw 8.8) Tohoku-Oki (2011, Mw 9.0)	Occurrence of very large earthquake and power-law size–frequency statistic	Visual correlation ; correlation	Level of theoretical tidal stresses		Ide et al., 2
Compressional (subduction)	Japan	Non-volcanic deep tremor and tremor rate	Statistical and modeling	Sea-level data and modeled ocean tidal stresses		Ide et al., 2
Compressional (subduction)	northern Cascadia Canada & USA	low-frequency earthquakes	Schuster test; SA	Theoretical tidal strain and stresses; sea-level data	*ST:* M2, N2, K2, K1, O1, P1, Q1, S2	Royer et al.,
Compressional (subduction) &Transform (after LE)	Kamtchaka, Russia; New Zealand (Mw≥6);	Aftershocks rate	Differential probability gain function	Modeled ocean tide height		Shebalin a Baranov, 2
Compressional (subduction)	Pacific ring	Occurrence of shallow earthquakes (<40 km)	Schuster test	Theoretical tidal stresses and ocean loading		Cochran et 2004

Table 14.1. List of selected studies that recognize a tidal influence on seismic activity in tectonic environments. Acronyms used: SA for spectral analysis (FFT-based technique); LE : large earthquake; *ST* and *LT* stand for short-term/long-term tidal constituents.* Includes 16 short- and 5 long-period tidal constituents.

Tectonic setting (period of activity)	Region	data	Method	Correlation with	Detected tides	References
All	Worldwide	Eruption occurrence	Schlien test	Theoretical solid tides + gravity data	*LT:* Mf	Mauk and Jonhson, 1973
Extensional (co-eruption)	Arctic sea, Pacific and Atlantic Oceans	Eruption occurrence	Schuster test	Ocean tide model	*LT:* Mf	Tolstoy, 2015
Extensional (co-eruption)	Holuhraun (Iceland)	Power radiated by lava field; seismic tremor	SSA	Length-of-day data	*LT:* MSm, Mm, Mf, Mt, Mtm, Msp,	Dumont et al., 2020
Intraplate (co-eruption)	Kilauea (Hawaii)	Eruption occurrence	Schuster test	Theoretical solid tides + gravity data	*LT:* Mf	Dzurisin et al., 1980
Intraplate (unrest)	Pico de Fogo (Cape Verde)	Seismic tremor and noise	SA	Sea-level data	*LT:* M2	Custódio et al., 2003
Intraplate (co-eruption)	Pico de Fogo (Cape Verde)	Lava volume flow rate; SO_2 flux; seismic tremor	SSA	Length-of-day and sea-level data	*ST:* P1, S2, M1, 2Q1, K1, N2/2"N2 *LT:* Mf/ MSf, Mt, Mtm	Dumont et al., 2021
Compressional (unrest)	Campi Flegrei (Italy)	Seismicity ; seismic noise and tremor; ground tilt; ground temperature ;	Statistical test (HiCum+ Schuster); ICA; SA; SSA	Theoretical solid tides ; Length-of-day data	*ST:* OO1, K1, M1, S1, P1, O1, K2, S2, M2, N2, S4 *LT:* Sa, Ssa, Mm, Msm, Mtm, Mt, Mf, Msf	Caputo et al., 2020; Petrosino et al., 2018; De Lauro et al., 2013, 2018; Cusano et al., 2021 Petrosino and Dumont, 2022
Compressional (co-eruption)	Stromboli (Italy)	frequency of small explosive events,	Schuster test + SA	Theoretical solid tides	*LT:* Mm, Msf, Mf	Sottili and Palladino, 2012
Compressional (co-eruption)	Etna (Italy)	Occurrence of explosive eruptions	Statistical +SA	Theoretical tidal acceleration	*ST:* quasi-diurnal, semi-diurnal, ter-diurnal	Sottili et al., 2007
Compressional (pre-eruption)	Ruapehu (New Zealand)	Seismic amplitude	Pearson test	Theoretical solid tides	*LT:* Mf	Girona et al., 2018
Compressional (co-eruption)	Miyake Jima (Japan)	Ground tilt, seismicity	Qualitative correlation	Theoretical tidal strain	*ST:* semi-diurnal, diurnal	Kasahara et al, 2001
Compressional (co-eruption)	Pavlof (USA)	Eruption occurrence	Qualitative correlation	Sea-level data	*LT:* Long ocean tides	McNutt & Beavan, 1987
Compressional (unrest & post-eruption)	Llaima and Villarrica (Chile)	SO2 flux	Cross-correlation + SA	Theoretical solid tides	*ST:* S2,S1,S3 *LT:* Mtm,fortnightly, MSm/Mm,	Bredemeyer and Hansteen, 2014

Table 14.2. List of selected studies that recognize a tidal influence in volcanic environments. Acronyms used: HiCum for Histogram cumulating (see Petrosino et al., 2018); SSA for Singular Spectrum Analysis; SA for spectral analysis (FFT-based technique); ICA for independent Component Analysis. *ST* and *LT* stand for short-term/long-term tidal constituents.

2.2 Methods to evaluate tidal influence on seismic and volcanic activity

Deciphering whether tectonic and volcanic activity is related to solid Earth and ocean tides amounts to evaluating the correlation between geophysical or geochemical observations on one hand and tidal time functions on the other hand. Several methods have been proposed to quantify the links (**Table 14.1 and Table 14.2**). More recently, these methods tend to combine both time and frequency-domain approaches (**Figure 14.2).**

Tidal time functions can be either theoretical or obtained from measurements, in which case they are referred to as time series. Numerous programs have been developed to model solid Earth and ocean tides. Thus, tidal acceleration can be calculated at a specific place on Earth for a specific time interval by using only the main or a selection of tidal constituents (see for instance Tanaka et al., 2012; Tolstoy et al., 2015; Petrosino et al., 2018). The tidal strains and stresses can be derived using *a priori* information on the orientation of geological structures. Continuous gravity measurements have been used to directly track the temporal evolution of the tidal acceleration at an observation site or in its direct vicinity (Dzurisin, 1980). Sea-level and atmospheric pressure data provide information on the tidal movements of the atmosphere and oceans (Custódio et al., 2003; Hillers et al., 2015; Royer et al., 2015; Caputo et al., 2020; Shebalin and Baranov, 2020; Dumont et al., 2021). In addition to these local parameters, one may also consider variations in the length-of-day (l.o.d.), which is a global parameter recorded daily on the Earth. The variations in l.o.d. record the acceleration and deceleration of the polar motion as a response to the redistribution of the solid and fluid masses on Earth, which mainly result from the lunisolar gravitational forces (see Le Mouël et al., 2019; Dumont et al., 2020, 2021; and chapter 17).

Most of the techniques commonly used to decipher tidal influence in geophysical data rely on statistical approaches**.** In the time domain, when testing the occurrence of individual events, such as earthquakes, the most widely used techniques are based on statistical tests (Emter, 1997 and references therein; **Figure 14.2)**. These methods first evaluate the distribution of geophysical events with respect to tidal cycles, which can either be a particular tidal cycle, or a cycle integrating several tidal periods. By splitting the cycle into regular bins, one can estimate the tidal phase, which represents the relative time of occurrence of the events with respect to two consecutive minima or maxima of the tidal time function. This analysis determines whether the distribution of events in time is uniform or whether events have a higher probability of occurrence during a specific portion of the tidal cycle, as shown by rose diagrams or histograms (**Figure 14.2)**. The significance of the non-uniform distribution can be assessed using a statistical test, the most common of which is the Schuster test, represented by a probability P (Emter, 1997 and references therein). Thus, for a given tidal cycle, events are considered non-random and the correlation is judged significant for a significantly

low P (< 5%). When dealing with continuous time series, like seismic amplitudes, gas fluxes or ground tilt data (see **Table 14.1 and Table 14.2**), the cross-correlation between geophysical and tidal time series allows for estimation of the correlation coefficient and time lag with respect to a specific tidal period (**Figure 14.2,** see Bredemeyer and Hansteen, 2014).

In the frequency domain, the detection of tidal periodicities in geophysical time series is mainly based on the Fourier Transform (FT). The resulting spectral peaks are then compared to the known or analyzed tidal periodicities (**Figure 14.2**). A number of variants of the FT exist, such as Welch's method, which employs moving time windows and enables the investigation of non-stationary periodic components in the data set (see, e.g., Emery and Thomson, 2014, for details). The Lomb-Scargle analysis was designed for time series with missing data points. Recently, spectral analysis based on the continuous wavelet transform has been preferred over classical methods, especially in the case of time series with non-stationary periodic patterns (Pering et al. 2019, and references therein).

While these methods provide a way to evaluate either the significance of oscillating patterns in time series or to characterize their spectral content, alternative methods that combine statistical and/or spectral analysis have gained interest in recent years. Examples of such approaches are the Independent Component Analysis (ICA) and the Singular Spectrum Analysis (SSA). ICA and SSA are both model-free methods allowing the separation of different components present in the time series. A time series can be viewed as a linear mixture of independent source signals, so ICA aims at finding a linear coordinate system from the data itself so that the components are statistically independent, assuming a non-Gaussian distribution (Hyvärinen and Oja, 2000). FastICA is the most widely used algorithm for performing ICA, converging particularly rapidly. Through an iterative procedure, FastICA maximizes a measure of non-Gaussianity of the data vectors to identify specific directions and hence the independent components (Hyvärinen and Oja, 2000). The decomposing approach of SSA is different, although it also relies on the hypothesis that extracted components are linearly related (Golyandina and Zhigljavsky, 2013). SSA belongs to the family of principal component analysis (PCA) techniques. It decomposes any time series into a sum of small number of components such as slowly varying trends, (pseudo) oscillations, and noise. The analysis is performed on a Hankel matrix built from lagged copies of the original time series that is then decomposed using the Singular Value Decomposition algorithm. It is the eigenvalues and associated eigenvectors that allow the identification of different components present in the original signal (Golyandina and Zhigljavsky, 2013). The pseudo-periodic components retrieved using SSA or ICA can then be compared with tidal ones using FT. These *ad hoc* methods (**Figure 14.2**) provide new insights by enabling the extraction of waveforms of tidal periodicities. For more details on application of these techniques, we refer the reader to De Lauro et al. (2018) and Dumont et al. (2020, 2021).

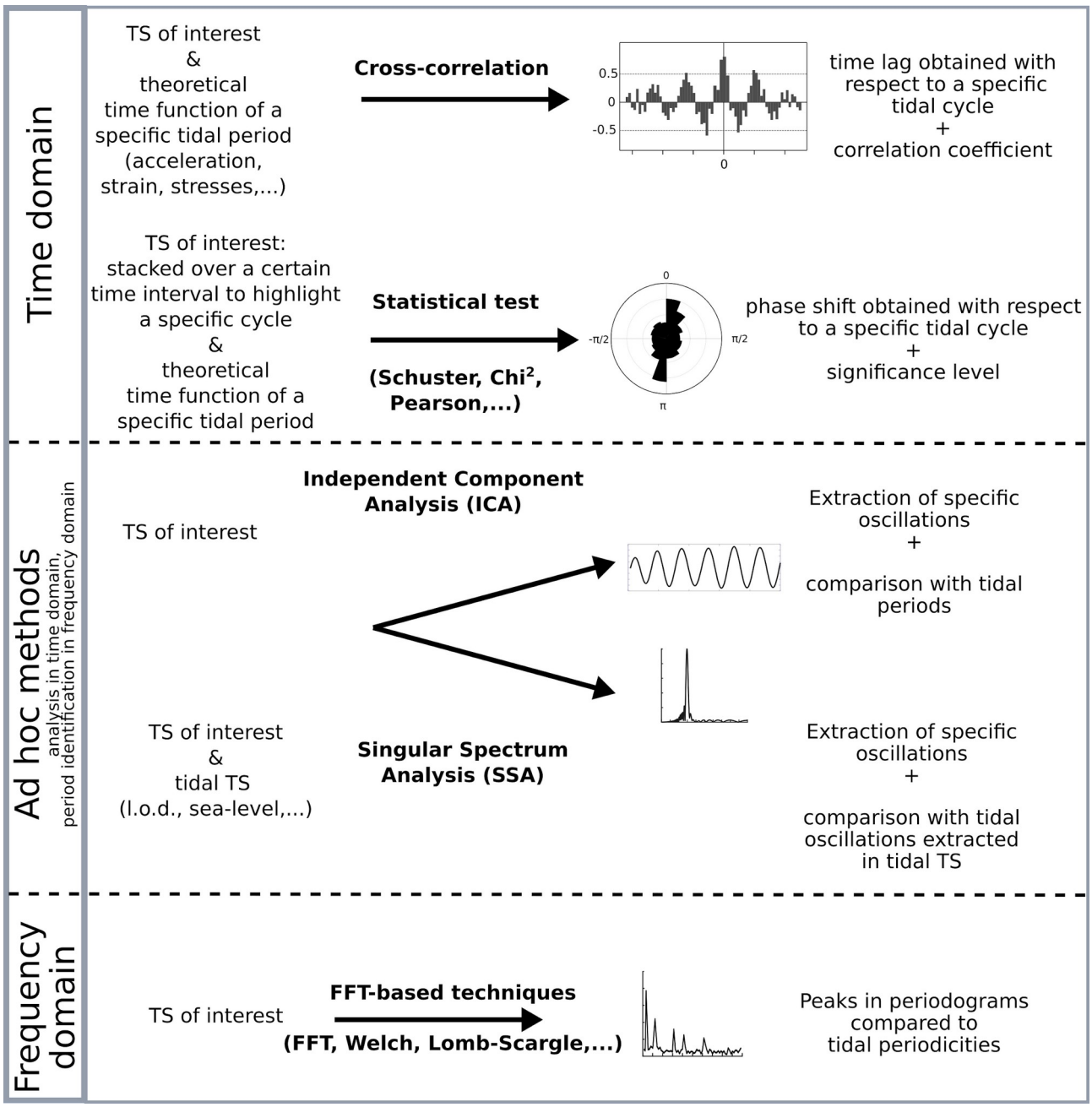

Figure 14.2: Summary of the different techniques used to assess the tidal influence on seismic and volcanic activity. TS stands for time series, and FFT for Fast Fourier Transform.

3. Case studies of tidal control on earthquakes and volcanoes

3.1. Tectonic systems

3.1.1. Continental Faults: The San Andreas Fault, California

The San Andreas fault (SAF) is an ~1,100 km continental transform fault that accommodates dextral displacements of up to 34 mm.yr^{-1} between the Pacific and North American plates (**Figure 14.1)**. Between 1857 and 1966, six intermediate magnitude (M~6) earthquakes occurred near the town of Parkfield, CA, with relatively regular inter-event times of ~20 years. These earthquakes ap-

pear to have ruptured the same or nearly the same fault area and, given their regularity, scientists estimated the time of the next earthquake occurrence and deployed abundant geophysical instrumentation in anticipation of future events. As such, the central section of the SAF is one of the most well instrumented fault segments in the world. The NW portion of the central SAF undergoes continuous fault motion, known as creep, and produces abundant microseismicity. Many of these events are characteristically repeating earthquakes that have nearly identical waveform and are thought to rupture the same fault area each time they occur. Additionally, the deep extension of the fault below the seismogenic zone hosts slow slip events, tectonic tremor, and LFEs (**Figure 14.3A and B)**.

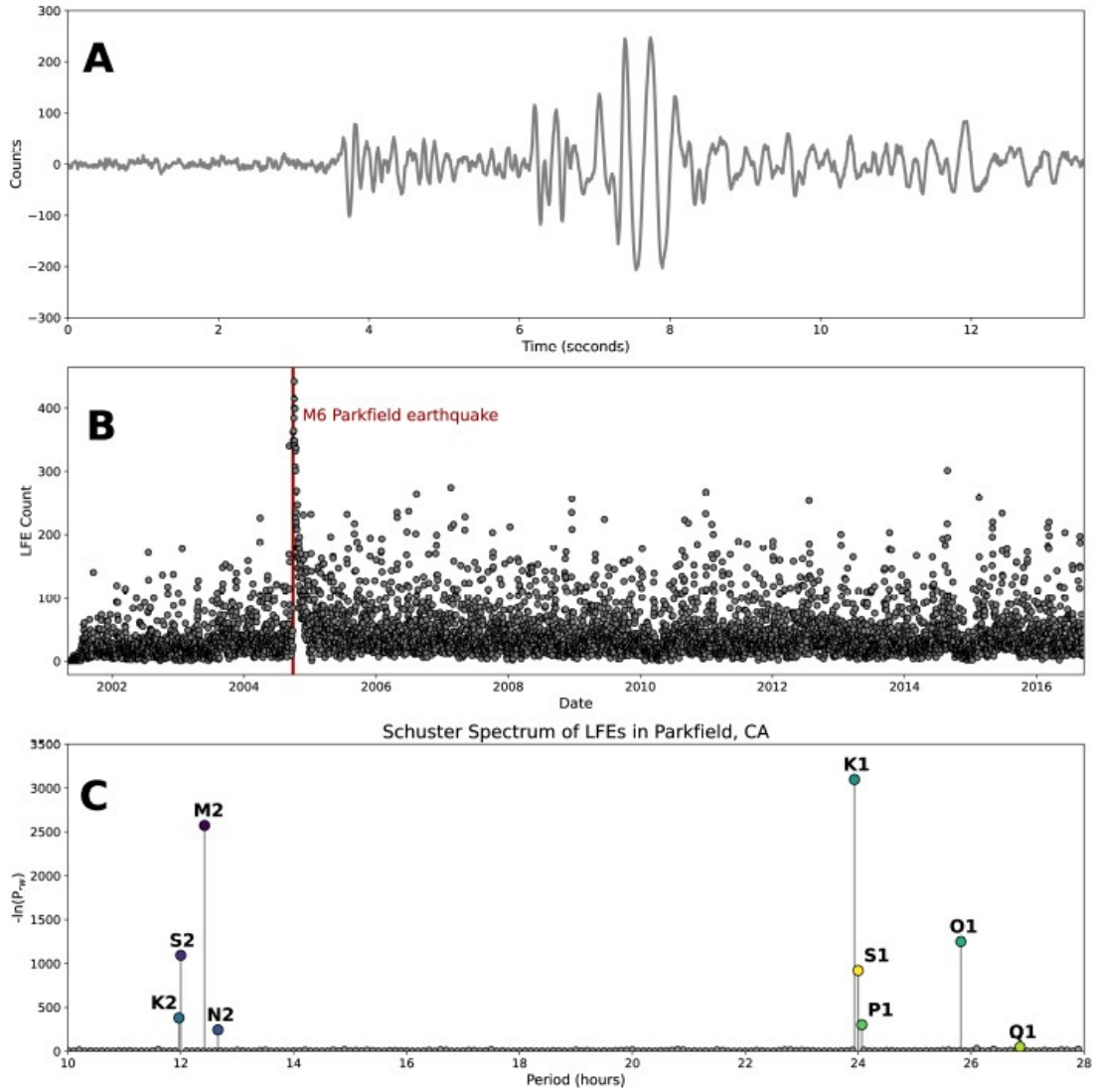

Figure 14.3: LFE waveforms, counts, and tidal sensitivity for the San Andreas Fault. A) Example of a LFE waveform. B) Daily LFE counts from the catalog of Shelly (2017). The catalog was declustered by considering only events that have repeat times greater than 15 minutes. C) Schuster spectrum of the daily number of LFEs with tidal constituents labeled, demonstrating a clear tidal control on the occurrence of LFEs.

Thomas et al. (2009) calculated the shear and normal stress changes on the SAF from both the body and load tides and explored the influence of these stress changes on the occurrence of non-volcanic tremor. They found that small magnitude shear stress changes of ~0.1 kPa had a strong

positive correlation with the rate of non-volcanic tremor. The largest magnitude tidal shear stress changes, i.e., those promoting shear slip on the fault, correspond to the largest tremor rates whereas the smallest magnitude shear stress changes, i.e., those discouraging shear slip, correspond to near-zero tremor rates. In contrast, fault normal stress changes that were more than an order of magnitude larger had only a very weak influence on tremor, promoting its occurrence solely at very large (~1.5 kPa) fault normal stresses. Later, LFEs were also identified on the deep SAF. These events are grouped into 88 different families based on waveform similarity and located at 16 -29 km depth along a 150 km section of the central SAF. A Schuster spectrum for the Parkfield LFEs is shown in **Figure 14.3C** below. Thomas et al. (2012) applied the same tidal stress analysis to each of the 88 families which allowed them to map the spatial variability of the tidal stress sensitivity. They found that all families were strongly influenced by tidal shear stresses, with positive shear stress correlating with rates as large as 2.5 times the average low-frequency earthquake rate. Most families were only sensitive to large magnitude fault normal stresses (large extensions), however, there were some spatial clusters that were more sensitive to normal stress changes (both positive and negative).

In summary, the observations show that normal stress changes of > 1kPa have little effect on the tremor and LFE rates, whereas much smaller magnitude positive (or negative) shear stress changes significantly increase (or decrease) the event rate. Slow slip, tremor, and low-frequency earthquakes are thought to occur in environments with extremely elevated, nearly lithostatic pore fluid pressures. Additionally, in deep fault zones porosity and permeability are extremely low, inhibiting fluid flow. Given these conditions, one explanation for the lack of sensitivity to normal stress changes is that changes in tidal normal stress are buffered by corresponding changes in pore fluid pressure (Hawthorne and Rubin, 2010). The low effective stresses also explain the sensitivity to tidal shear stress. Seismicity rate modulation depends on the ratio of the tidal shear stress amplitude to the effective stress. While the shear stress amplitudes are generally low, the low-effective stresses present in these deep faulting environments amplify their effects. A similar modulation of LFE activity has also been reported in the Cascadia Subduction Zone (Royer et al., 2015), and Japan, suggesting that these interpretations extend to LFEs in diverse tectonic environments.

3.1.2. Subduction Zones: Japan

Japan sits above two of the most seismically active subduction zones in the world (**Figure 14.1**). In the northeast, the Pacific plate subducts below the north American plate, whereas to the southeast the Philippine Sea plate plunges below the Eurasian plate. Japan hosts a variety of seismic events, such as mega-thrust earthquakes, intraplate earthquakes, slow slip events and non-volcanic tremor, in addition to tectonic volcanism. The seismic activity is extremely well recorded owing to the presence of the densest and highest-quality regional seismic networks in the world, including Hi-Net, K-Net, KiK-Net, F-Net, and seafloor sensors established after the 2011 Tohoku earthquake.

The high-quality instrumentation in Japan together with the high rates of seismic activity have allowed for careful studies of the impact of tides on the seismicity. Tanaka et al (2004) investigated the possible tidal control of shallow (≤ 70 km) earthquakes using 89,505 events recorded between

1997 and 2002. They hypothesized that tidal stresses could promote earthquakes if they acted in the same direction as regional tectonic stresses, thus enhancing the tectonic load. To quantify the tidal forcing, the authors calculated the tidal stress tensor for the hypocenter and origin time of each earthquake by considering both the solid Earth tides and tidal ocean load tides. The horizontal projection of the maximum compressive stress was computed, which was considered as the tidal azimuth. The same procedure was then repeated for synthesized random earthquake distributions. The authors found insignificant correlations between Earth tides and earthquake occurrence for most regions but identified a significant correlation between areas of recent unusual tectonic activity and places where future large earthquakes were expected.

The idea that specific regions could become more sensitive to tides around periods of enhanced seismic activity was further explored in subsequent studies. Tanaka (2012) investigated 541 earthquakes of Mw>5.0 that occurred in the 35 years preceding the 2011 Mw9.1 Tohoku earthquake. The author started by computing the tidal stresses, including both the solid Earth tides and ocean load tides, at the epicentral location, depth and origin time of each earthquake. The tidal stresses were then projected onto the fault plane of each individual earthquake based on its focal mechanism. A tidal phase angle was assigned to each event, with phases of 0˚ and ±180˚ corresponding to earthquakes occurring at times of tidal stress maxima and minima, respectively. A Schuster test was used to assess the probability that the tidal phase distribution was non-random. The study found no significant tidal control when all events in the area were considered. However, a clear tidal control was detected if only earthquakes in the hypocentral area of the Tohoku earthquake were considered. The analysis showed that in the decade preceding the Tohoku earthquake, the sensitivity to tides gradually increased in the hypocentral region of the mega-thrust earthquake, with events preferentially occurring at times when tidal stresses promoted failure the most. The tidal sensitivity disappeared after the occurrence of the Tohoku earthquake. These results suggest that the hypocentral area of the Tohoku earthquake became more sensitive to tidal stresses as it became critically stressed in the precursory stage leading to the main shock.

Further evidence of tidal control on seismic activity in Japan comes from the analysis of deep non-volcanic tremors. Ide et al (2014) studied, in detail, the Okayama tremor cluster and showed that the number of tremors had a clear tidal modulation over 9 years of observations, with tremors only occurring when ocean tides were at a low level. The authors proposed that the occurrence of tremors is facilitated by the unclamping of the subduction interface at low tide levels. At these times, the ocean load is decreased, the normal stress on the plate interface decreases, and the shear stress increases, promoting shear slip. Based on these observations, the authors proposed an empirical non-linear relationship between stress (tidal level) and slip (tremor rate). They then used the inferred empirical relationship to predict the number of tremors in the previous 50 years. Although a catalog of tremors only exists for recent years, the predicted tremor rate is in agreement with the catalogued background seismicity rate. Hence, the authors suggested that tidal stresses drive deep plate motion, which in turn loads the entire plate interface, modulating both tremor and background seismicity.

3.2 Volcanic settings

3.2.1 Unrest calderas: The hydrothermal system of Campi Flegrei, Italy

The Campi Flegrei volcanic complex is located west of Naples, Southern Italy (**Figure 14.1**). It results from the subduction of the African plate underneath the European lithosphere. The caldera formed after two major collapses, the Campanian Ignimbrite (~39 kyrs) and the Neapolitan Yellow Tuff (~15 kyrs). Following the latter major collapse, more than 60 eruptions occurred within the caldera which presently consists of a ~13 km-diameter partially submerged depression. The most recent eruptive centers, including the Solfatara crater, were active between 4.8 and 3.8 kyrs, while the last eruption occurred in 1538 A.D. and formed the Monte Nuovo cone. In recent decades, the central sector of the caldera has undergone regular bradyseisms, which consist of alternating phases of fast ground uplift and slow subsidence. Uplift episodes are accompanied by volcano-tectonic seismicity and seismic swarms as well as less frequent long-period earthquakes. Most seismic events are located at shallow depths (<4 km) beneath the Solfatara crater, which is also characterized by intense hydrothermal activity, boiling mud pools and diffuse degassing. The most recent and major bradyseismic crises occurred in 1969-1972 and 1982-1984. Two main hypotheses have been developed to explain such pattern of ground deformation: 1) pressurization of a gas reservoir at 3–4 km depth, above a deeper magma body; and 2) repeated CO_2-rich fluid injections from the magma reservoir into the hydrothermal system located in the first 2 km of the crust. A new phase of ground uplift began in 2005.

Tidal modulation of volcanic activity was first discovered at Campi Flegrei in the 1990's (Berrino and Corrado, 1991). Since then, periodicities ranging from semi-diurnal to annual have been identified in various geophysical parameters (**Table 14.2**). Additional studies have highlighted tidal influence during the ongoing unrest (Petrosino et al., 2018; Petrosino and Dumont, 2022; Cusano et al., 2021) allowing to further decipher the interaction between the dynamics of Campi Flegrei caldera and solid Earth tides; note that the ocean tide is quite small in the Mediterranean sea (Ray and Erofeeva, 2014).

De Lauro et al. (2018) applied an ICA on ground tilt data recorded between 2015 and 2019 at Campi Flegrei to show that ground in the central part of the caldera was oscillating at tidal frequencies. Besides the overall trend related to internal processes, e.g., uplift of magmatic and/or hydrothermal origin, the ground tilt time series contains variations, also detected along specific ground tilt azimuths, whose frequencies coincide with that of diurnal (S1), fortnightly (Mf) and lunar monthly (Mm) tidal constituents (**Figure 14.4A**). These directions of tilting correspond to that of pre-existing structural features located within the caldera. In addition, the amplitude variations of these tidal constituents were interpreted as "site effect", e.g., an amplitude modulated by the properties of the underlying rock layers. These observations reveal that the response of ground tilt to solid Earth tides is an oscillatory behavior of small-scale modulated by the local stress field, tectonic structures, and geology.

Further evidence of tidal forcing at Campi Flegrei comes from the spectral analysis of ground temperature measurements performed at sites of intense fumarolic activity in the Solfatara crater (Caputo et al., 2020). Lunisolar and synodic fortnightly (Mf, Msf), lunar and solar monthly (Mm, Msm), and solar semi-annual and annual (Ssa, Sa) components appear in the time series

recorded by infrared cameras installed in different areas between 2014 and 2019 (**Table 14.2 and Figure 14.4B**). The solar annual and semi-annual constituents have almost comparable amplitudes and do not depend on the observation site, indicating a similar response of the ground temperature to longer-period tidal strains. On the other hand, the amplitudes of the monthly and fortnightly periods show some slight differences (**Figure 14.4B**), suggesting that the response of the sub-surface to solid Earth tides may be influenced by local site effects in sites where intense fluid circulation takes place, similar to what is observed for ground tilt.

The results of De Lauro et al., (2013) and Petrosino et al., (2018) indicate that both hydrothermal tremor and seismicity in Campi Flegrei are modulated by solid Earth tides. The hydrothermal seismic tremor consists of polarized vibrations whose spectrum have peaks corresponding to lunisolar diurnal (O1, M1, K1, S1) and semi-diurnal (S2) periodicities (De Lauro et al., 2013). The authors observed that the lunar contributions (O1, M1, and K1) became predominant in 2006, when fluid was injected from the geothermal reservoir into the shallower hydrothermal system of Solfatara crater. With similar observations made for the past bradyseismic crises of 1969-1972 and 1982-1984, it appears that the enrichment of tidal constituents in the spectra of the geophysical time series represents a marker of unrest episodes (De Lauro et al., 2013 and references therein). Moreover, these movements of fluids may generate vibrations that are known as long-period (LP) earthquakes. The energy released by LP earthquakes shows a cyclic pattern that coincides with that of the diurnal solid Earth tide. This behavior was ascribed to tidally-modulated fluid recharge/discharge in the fractures of the hydrothermal system, which in turn responds by generating LP events at similar frequencies but of varying energy.

Volcano-tectonic (VT) earthquakes are either caused by slip along faults or by pressure changes induced by magma transfer near or within a volcanic system. Petrosino et al., (2018) showed that the rate of clustered VT events was clearly modulated by solid Earth tides during the 2005-2016 interval. Their statistical analysis indicates that the events belonging to seismic clusters do not occur randomly in time; instead, they are significantly correlated - above the 95% confidence level - with a large number of periods corresponding to tidal constituents including the lunisolar semi-diurnal, diurnal, fortnightly, monthly, semi-annual and annual periodicities (**Table 14.2 and Figure 14.4C-D**). Such oscillatory behavior is not observed for the background VT events. These results suggest that tidal forces interfere with crustal processes by enhancing or restraining crustal deformation, stress buildup and fluid movements, thus modulating the opening and closure of voids. By driving changes in the crustal permeability, solid Earth tides alter the internal pressure of rocks, eventually promoting earthquake triggering.

In summary, these studies demonstrate that, at the Campi Flegrei caldera, the tidal influence happens through a complex coupling mechanism that affects both the crustal structure and hydrothermal fluids, suggesting a synchronization between Earth tides and magmatic and hydrothermal activity on both short and long terms. The tidal influence is particularly remarkable during phases of unrest, when the caldera is close to unstable conditions, which seem to make the volcanic system more sensitive to tidal forcing.

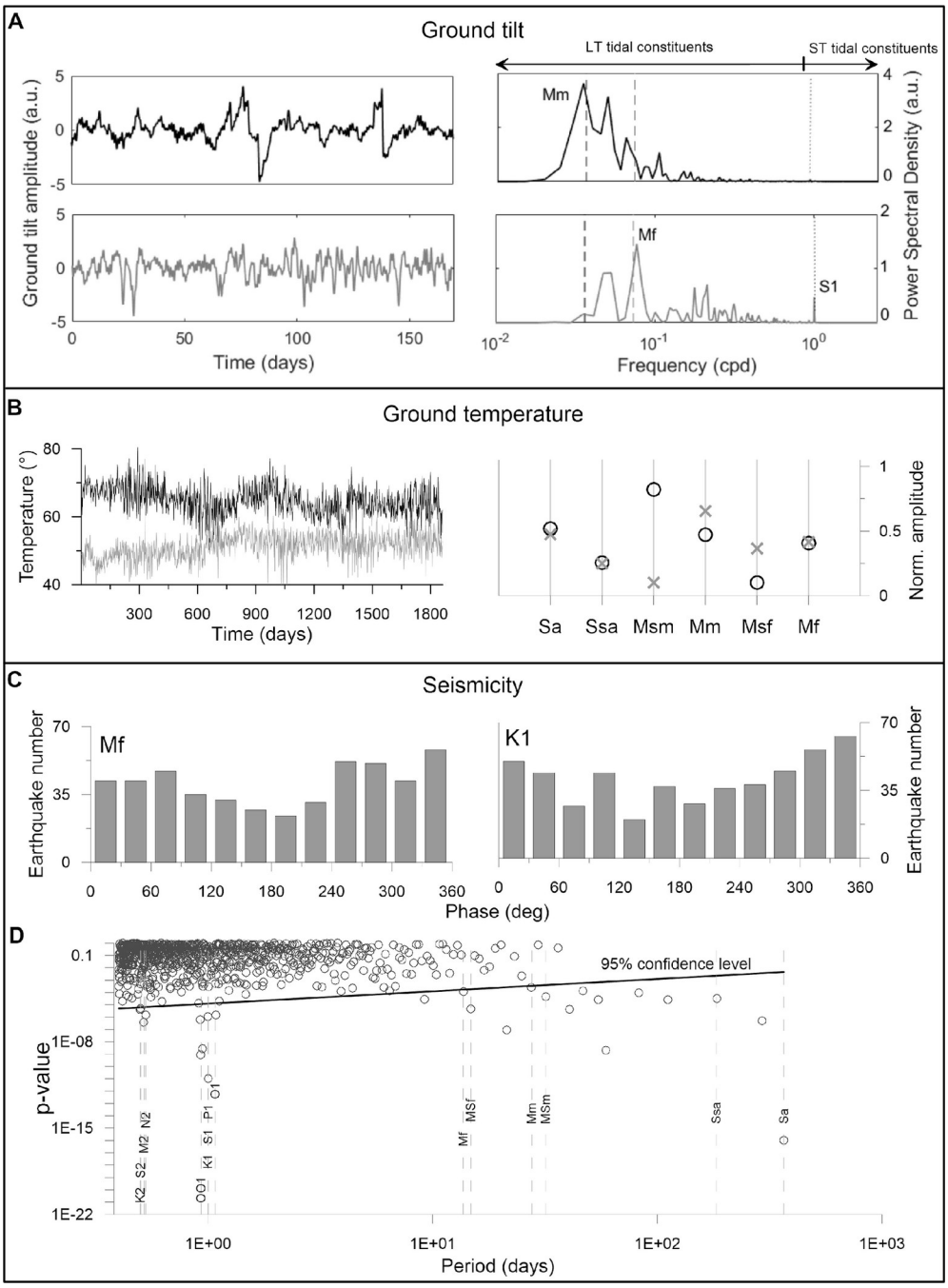

Figure 14.4: Tidal influence on various geophysical parameters observed at the Campi Flegrei caldera. A) On the left, independent components mainly associated with Mm (black curve) and Mf (gray curve) extracted by ICA from ground tilt data recorded in 2015-2019 and the corresponding power spectral density PSD (right). LT and ST stands for Short and Long-term. Modified from De Lauro et al., 2018. B) Ground temperature variations recorded in 2014-2019 by two infrared cameras deployed in the Solfatara crater (left) and associated tidal constituents identified by spectral analysis (right). Modified from Caputo et al., 2020. C) Frequency distribution of earthquake occurrence for the 2005-2016 period analyzed with respect to the Mf and K1 phases. D) Schuster spectrum calculated over the 2005-2016 earthquake catalog for tidal periods ranging from 0.4 to 366 days. p-values exceeding the 95% confidence level indicate a non-random distribution. The dashed vertical lines correspond to the main tidal periods. (C-D) Modified from Petrosino et al., 2018.

3.2.2 Erupting volcanic systems: Short to long-term tidal influence

Following an eruption onset, magmatic fluids are emitted at the surface in different ways that determine the eruptive style, where purely effusive and explosive behaviors are the two end-members. Similar to hydrothermally active volcanoes, magmatic fluids can be tracked in space and time, with the difference that the emission of eruptive products at the surface can be monitored using a larger variety of ground, air and satellite-based sensors. In fact, the use of multi-method data has largely contributed to deciphering the dynamics of volcanic eruptions, by correlating visual observations with geophysical and geochemical signals (Geshi et al., 2002; Aiuppa et al., 2010; Gudmundsson et al., 2016).

In August 2014, the eruption of Holuhraun in central Iceland (**Figure 14.1**), began, at ~10 km north of the largest glacier in Europe. This effusive eruption lasted six months and produced a lava field with a volume of ~1 km^3 (Dumont et al., 2020 and references therein). The growth of the lava field was captured by satellite measurements through the thermal energy it radiated over the course of the eruption. Together with seismic tremor, the satellite data was analyzed using SSA (**Figure 14.5A**, Dumont et al., 2020). The authors identified up to 8 tidal periods in each time series, varying between ~5 and ~32 days and corresponding to periods of Earth tides, as confirmed by the analysis of l.o.d. variations (**Table 14.2**). They showed that these tidal periods represent ~50% of both geophysical time series. In addition, the reconstruction of the two time series based on trends and tidal periods explains most of the variations in the original signals (**Figure 14.5A**). Similar results were obtained for the 2014-2015 eruption of Fogo volcano, Cape Verde (Dumont et al., 2021). These studies have shown that movements of magmatic fluids - gas, melt and lava - from the upper crust to the Earth's surface and atmosphere, are all modulated by a combination of solid Earth tides.

In the Aeolian Islands in Italy (**Figure 14.1)**, long-lived activity at the Stromboli volcano has been characterized by jet-like explosions over the past 1300 yrs (Taddeucci et al., 2013). Yearly to daily fluctuations in seismicity, thermal emissions, deep gas influx and frequency of strombolian explosions are often associated with crater overflow, lava flank eruptions and episodic, moderate-to-large strombolian explosions. However, Sottili and Palladino (2012) showed that the occurrence of explosive events at Stromboli volcano are also modulated by solid Earth tides. Their statistical analysis relies on the hourly number of explosive events as identified by Very Long Period (VLP) seismic events that they generate, and which includes ~150.000 events over a 17-month period (**Figure 14.5B**). The analysis shows that the frequency of explosive events increases by more than 85% during fortnightly tidal maxima. These results suggest that in open-conduit volcanoes of mafic composition like Stromboli, the fortnightly tide can induce cycles of compression–decompression of wall rocks. These pressure variations in turn modulate the escape of magmatic volatiles and fluid-driven cracking of the country rocks, and the final transfer of magma in the upper crust and volcanic conduit (Sottili and Palladino, 2012).

Solid and ocean Earth tides have been evoked to influence the triggering of volcanic eruptions. As an example, Dzurisin (1980) analyzed the timing of 52 historical eruptions that occurred since the first half of the nineteenth century at Kilauea volcano, Hawaii (**Figure 14.1)**, with respect to the vertical component of the lunisolar synodic fortnightly solid Earth tide. The study revealed

that the onset of 34 of the 52 historical eruptions took place within 3 days prior or after a fortnightly maximum (89% confidence level), which corresponds to an eruption probability 1.9 times greater during tidal maxima than during minima (**Figure 14.5C**). The causal relationship between tidal maxima and onsets of historic eruptions at Kilauea was attributed to the enhancement by solid Earth tides of already existing volcano-tectonic stresses. Such a correlation was not observed for Mauna Loa, another volcano located on the same island, for which 37 historical eruptions were similarly analyzed. This difference in the response of neighboring volcanoes to tidal forcing was attributed to the different structures and/or plumbing system of the two volcanoes.

The influence of ocean tides and associated loading has not only been demonstrated on submarine volcanic systems (Tolstoy, 2015), but also on volcanoes located in coastal regions. McNutt and Beavan (1987) showed that the number of monthly volcanic eruptions at Pavlof volcano, Alaska (**Figure 14.1**), including both magmatic and explosive eruptive events, is much higher in fall and winter (**Figure 14.5D**). This volcanic activity appears to be correlated with variations in sea-level, which are either rising or close to a maximum during these two seasons (**Figure 14.5D**). A rising sea-level corresponds to a larger ocean loading on the volcanic system, resulting in the extrusion of magma. They also showed that this correlation is clearer for long-period (>8 months) variations of sea-level. The authors explain this behavior by suggesting that the different portions of the magma plumbing system of Pavlof volcano, associated with different rheological behaviors, may respond differently to tidal oscillations of different periods and related pressure variations.

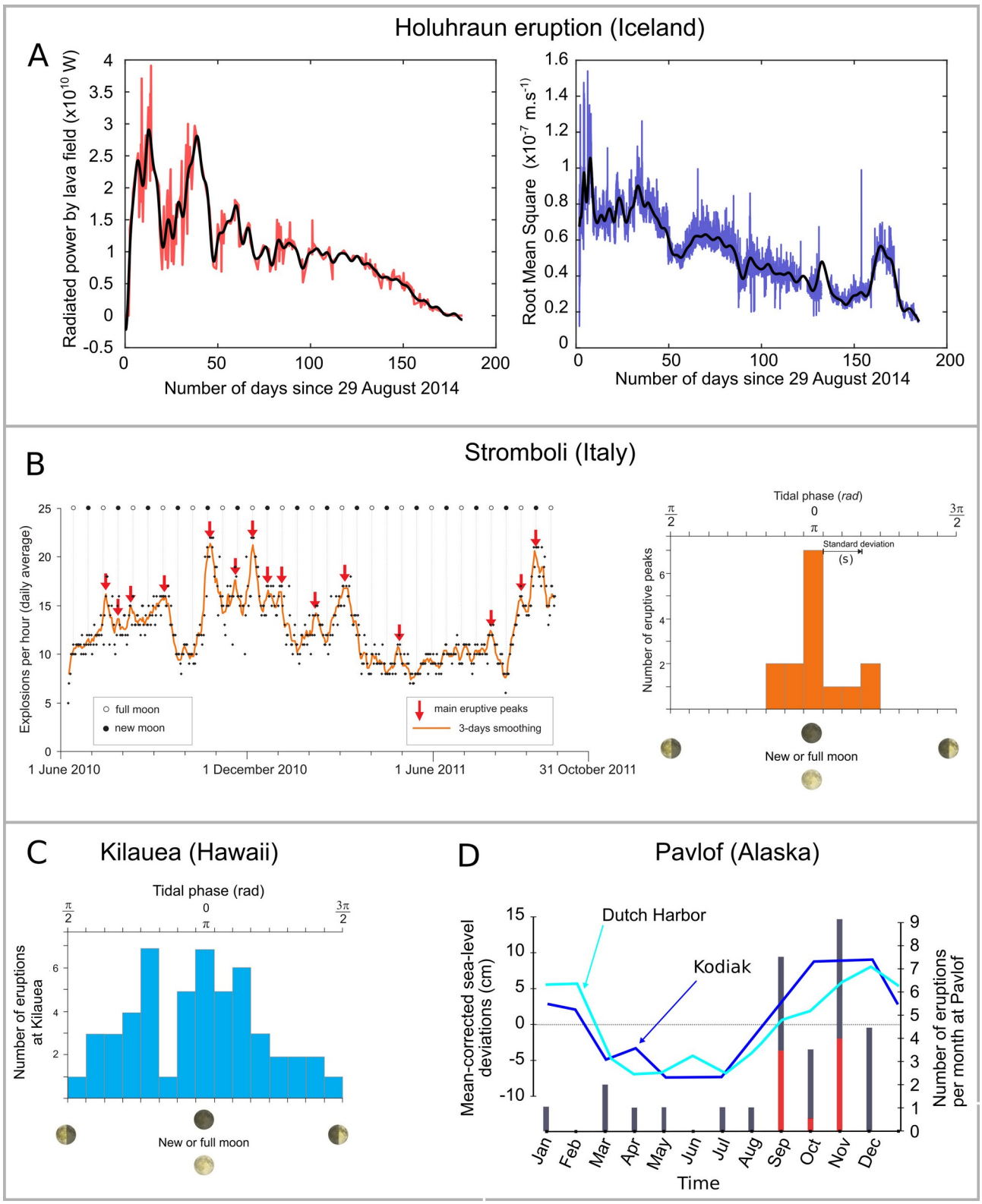

Figure 14.5: Tidal influence at erupting volcanoes. A) Power radiated by the lava field (red) and seismic tremor (blue) recorded during the 2014-2015 Holuhraun eruption (Iceland) and their reconstruction (black) using tidal constituents. Modified from Dumont et al., (2020). B) (Left) Number of explosive events per hour (EH) recorded for each day between June 2010 and October 2011. The EH curve (orange) smoothed over a 3-day time windows shows 15 main positive peaks at ~14-day intervals or multiples, concomitant to the fortnightly Earth tide maxima. (Right) Histogram of the

main 15 peaks of hourly explosions represented as a function of the fortnightly tidal phases. The phase increment is 12º, with 24º of tidal phase corresponding to 1 day. Modified after Sottili and Palladino (2012). C) Histogram showing the eruption onset at Kilauea volcano with respect to the Mf fortnightly tide. Drawn after Table 1 from Dzurisin (1980). D) Deviations from monthly mean sea-level variations (blue curves) estimated for two tide gauges, Kodiak and Dutch Harbor located ~350 and ~500 km from Pavlof volcano, and for the period 1950-1974. The number of monthly explosive (gray bars) and magmatic (red bars) eruptions is stacked over the 1973-1984 period. Redrawn from McNutt and Beavan (1987).

4. How do tides influence seismic and volcanic activity?

Previously, we showed that a large variety of data sets acquired in the vicinity of fault and volcanic systems reveals tidal components with periods ranging from semi-diurnal to (multi-) annual (**Table 14.1** and **Table 14.2**). As explained in chapters 4 and 15, the stronger tidal amplitudes are primarily found for the passage of the Sun and Moon over short periods, being of the order of 24000, 11000, 9800 and 4600 cm^2/s^2 for M2, S2, O1 and P1, respectively. For diurnal and longer periods, variations of the Moon declination, which lead to Mf or K1 tides, become predominant, with amplitudes of ~6500 and ~13900 cm^2/s^2, respectively (Ray and Erofeeva, 2014), explaining why these tidal constituents are among the most commonly detected worldwide (**Table 14.1** and **Table 14.2)**.

Tidal forcing is more noticeable on the fluid envelopes of the Earth, but as outlined above, they affect the solid Earth as well. The elastic response of the Earth to such external forcing is given by the Liouville-Euler equations (Lambeck, 2005; Lopes et al., 2021; and chapter 15). These equations allow to evaluate the redistribution of the mass and stresses at the surface of the solid Earth, due to tides. Such phenomena directly impact the dynamics of our planet. Although tidal stresses have been estimated to be 2-3 orders of magnitude lower than the fault strength, their action influences dynamical systems such faults and volcanoes. Both faults and volcanoes are characterized by low-tectonic or magmatic stressing rates over hundreds of years before they reach their failure threshold and earthquakes or eruptions are triggered. In submarine and coastal geological systems, the load of ocean tides are superimposed on the solid Earth tides. Ocean tides and so loading have similar frequencies to those of solid Earth tides, in addition to some others that are specific to ocean currents.

The way tectonic and volcanic systems accommodate strain and stresses depends on their internal properties (composition, pore-fluid saturation, friction) and structure (Mauk and Jonhson, 1973; Dzurisin, 1980; McNutt and Beavan, 1987; Royer et al.,2015; Hillers et al., 2015; De Lauro et al., 2018; Malagnini et al., 2019). The geometry of geological systems, such as orientated planes or complex volumes, governs their deformation and makes them more sensitive to certain types of tidal stresses such as volumetric strains, shear or normal stresses, as particularly well illustrated by the studies of Thomas et al. (2009) for the San Andreas fault and of Sottili et al. (2007) for the Etna volcano. Recently, a new approach has been proposed to further characterize the specific response of a geological system to tidal forcing. Dumont et al., (2021) identified tidal periodicities in three geophysical time series acquired during the 2014-2015 eruption at Fogo volcano, Cape Verde. Based on these tidal frequencies, the authors estimated the transfer function corresponding to the re-

sponse of the volcano to tidal potential. They showed that during the eruption the volcano behaved as a bandpass filter to tidal forcing, being more sensitive to specific periods, those above one day, such as those of Q1, and up to ~9 days (**Figure 14.6**).

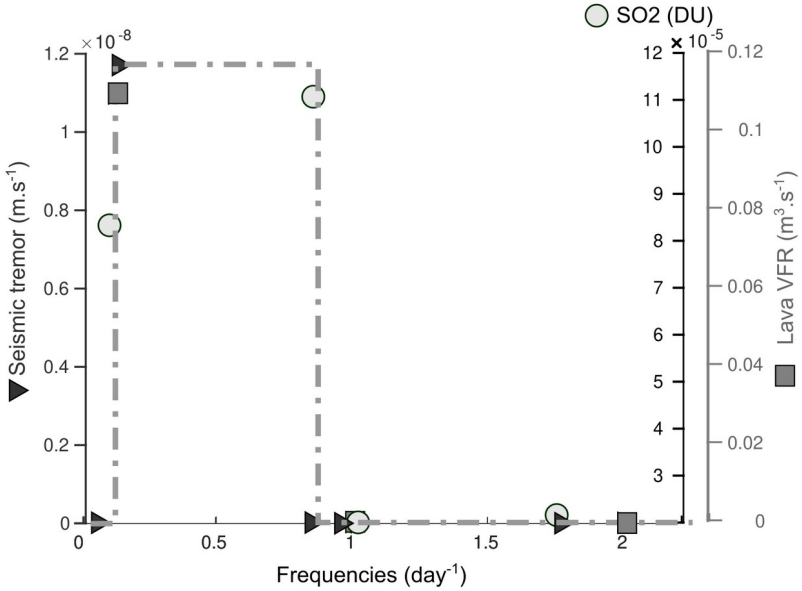

Figure 14.6: Amplitude associated with tidal components extracted in the three volcanological time series acquired during the 2014-2015 Fogo eruption, Cape Verde, and represented as a function of their frequency (in day^{-1}). The three time series are the seismic tremor (dark gray triangle), the SO_2 emission (light gray circle, DU for Dobson unit) and lava volume flow rate (VFR, gray square). This representation reveals that the volcano acts as a bandpass filter to tidal components showing sensitivity in the frequency band ~0.1 to 0.85 days^{-1}. Modified after Dumont et al. (2021).

Beyond compositional and structural aspects, sensitivity to tides seems also to increase for some faults and volcanoes when they are in a critical stress state, approaching failure conditions (Tanaka, 2012; Girona et al., 2018; Malagnini et al., 2019; Petrosino et al., 2018) or following stress release (Malagnini et al., 2019; Shebalin and Baranov, 2020). The small tidal stress variations and in particular their rate, which may exceed that of tectonic and volcano-tectonic stresses, ~10 hPa/hour versus ~0.2-1.5 hPa/hour (Emter, 1997), can accelerate the destabilization of dynamical systems.

Finally, the movement of fluid masses as a response to lunisolar gravitational forces is not reduced to the stresses they exert on geological systems. Fluids are pervasive throughout Earth's crust, below the water table. Tides can alter pore-fluid pressure in rocks either promoting or impeding failure, as described by the Coulomb failure criterion (Scholz, 2019). Fluids are also omnipresent at volcanoes from multi-phase fluids (melt, crystals, gas), hydrothermal fluids to extruded lava. Tidal forcing can drive fluid motion in both hydrothermal and magmatic systems. Their modulation by solid Earth tides is observed from the upper crust to the Earth surface, as well as in the atmosphere, and mainly during eruptions that are dominantly effusive.

5. Summary and future outlook

The once debated influence of tides on seismic and volcanic activity is now firmly established. In this chapter, we summarized the types of data that can be used to characterize seismic/volcanic activity and tidal forcing. The geophysical parameters that respond to tidal forcing include the number and rate of earthquakes, LFEs, and LPs, tremor amplitudes, variations in attenuation, power radiated by lava fields, eruption occurrence, lava flow rate, SO_2 and radon fluxes, ground tilt and ground temperature, among others. Tidal variations and components can be estimated numerically from theoretical computations or from measurements of gravity, atmospheric pressure, sea-level, l.o.d., and other parameters. The methods used to identify the tidal influence on geophysical parameters can be divided into time-domain correlations and statistical tests, which assess the similarity between data sets (e.g., Schuster, Chi-squared, Pearson or Kolmogorov-Smirnov), frequency-domain methods that allow for characterization of the periodicities of the data sets (e.g., FT, Welch, Lomb-Scargle), and *ad hoc* methods (e.g., ICA, SSA), which have become more popular in recent years for harnessing the power of both types of analyses.

The tidal modulation of seismic and volcanic activity has been observed in a variety of settings around the world. Here, we summarized some key observations in example study regions. In a continental setting, the central section of the San Andreas fault, in California, shows a clear tidal modulation of both tremor rates (Thomas et al, 2009) and number of LFEs. Notably, tremor on the SAF is more sensitive to shear tidal stresses than to normal shear stresses, which can be interpreted as a marker of low effective stresses in a deep fault environment, where changes in normal stresses are buffered by changes in pore fluid pressure (Thomas et al, 2009). Tremor is also commonly observed in subduction zones. As an example, a clear tidal modulation is observed for some of the non-volcanic tremor observed in Japan (Ide et al., 2014). In particular, an empirical non-linear relationship was proposed to relate stress (tidal level) to slip (tremor rate). Remarkably, the same relationship was effective at predicting the background seismicity rate over 50 years of observations, suggesting that tidal stresses influence deep plate motion, therefore controlling activity along the whole plate interface. Hydrothermal systems are often prone to the influence of tides. One such example is Campi Flegrei in Italy. Here, both ground tilt and ground temperature show clear tidal periodicities. The influence of short-term tidal constituents on ground deformation varies from site to site, suggesting that site effects strongly control their influence. The long-term tidal constituents equally affect all observations, suggesting that the mechanism sensitive to long-term tidal forcing is not local. In the fluid-rich environment of Campi Flegrei, the fluid charge/discharge in the fractures of the hydrothermal system also responds to tides, as shown by the tidal modulation of tremor and LP events. Magmatic systems at active volcanoes are also strongly sensitive to tides, as shown for Holuhraun (Iceland), Fogo (Cape Verde), Stromboli (Italy), Kilauea (Hawaii) and Pavlof (Alaska), among others. The observations suggest that magma plumbing systems respond differently to tidal forcing with greater responsiveness for their fluid components.

While the existence of tidal controls on seismic and volcanic activity around the world is now demonstrated beyond doubt, the conditions under which it occurs remain a matter of debate. In fact, the observations suggest that tidal forcing only becomes effective under specific conditions, explaining the contradictory results in past studies. Some systems, both tectonic and volcanic, become sensitive to tidal forces just around times of enhanced activity, either shortly before or after eruptions or major earthquakes (Tanaka, 2012; Girona et al., 2018). This key observation suggests that

systems may become more sensitive to the low-magnitude tidal stresses as they enter a critical state. Importantly, this implies that tidal sensitivity might potentially be used in earthquake and volcano monitoring. Other systems show a tidal sensitivity that depends on the orientation of volcano-tectonic stresses and/or fractures, again suggesting that tidal forces are only effective when they work to enhance the already-existing stresses in the geophysical systems. Notably, some systems seem to be sensitive only to specific tidal constituents.

The decisive factor that made the existence of tidal controls on seismic and volcanic activities clear was the increase in the quantity and quality of observations, particularly observations that are high resolution in space, time, or both. As our observational capability continues to increase, new studies will allow better characterization of quiescent states and their transition into periods of increased seismic and volcanic activity. Such observations can also be used to determine both the conditions that make a geological system sensitive to certain tidal periodicities and the interplay between internal and external processes that take place on short and long timescales that may lead to the triggering of earthquakes and volcanic eruptions. Numerical modeling will facilitate testing of conceptual and theoretical models, leading to a better understanding of the dynamics of these systems.

Acknowledgments:

The authors thank the editors Mattias Green and João C. Duarte for their invitation to contribute to this book and D. Schlaphorst for his feedback on the chapter. SD also thanks F. Lopes for fruitful discussions during the chapter writing. SD acknowledges the Fundação para a Ciência e Tecnologia (FCT) and the European Union (UE) for their financial support through the fellowship SFRH/BPD/117714/2016, co-financed by the Ministério da Ciência, Tecnologia e Ensino Superior (MCTES), Fundo Social Europeu (FSE), and Centro 2020. This work was funded by the projects PTDC/CTA-GEF/6674/2020 - RESTLESS and UIDB/50019/2020, Instituto Dom Luiz (IDL) funded by FCT.